How to cite: Angew. Chem. Int. Ed. 2024, e202410857
doi.org/10.1002/anie.202410857

Organic Solar Cells Hot Paper

Non-Ionic Perylene-Diimide Polymer as Universal Cathode Interlayer for Conventional, Inverted, and Blade-Coated Organic Solar Cells

Luxin Feng[+], Yanhe Xiang[+], Zhe Li, Qingyang Li, Hongliang Dong, Shouke Yan, Bowei Xu, and Jianhui Hou**

Abstract: As a class of predominantly used cathode interlayers (CILs) in organic solar cells (OSCs), perylene-diimide (PDI)-based polymers exhibit intriguing characteristics of excellent charge transporting capacity and suitable energy levels. Despite that, PDI-based CILs with satisfied film-forming ability and adequate solvent resistance are rather rare, which not only limits the further advance of OSC performances but also hinders the practical use of PDI CILs. Herein, we designed and synthesized two non-conjugated PDI polymers for achieving high power conversion efficiency (PCE) in diverse types of OSCs. The utilization of oligo (ethylene glycol) (OEG) linkage enhanced the n-doping effect of PDI polymers, leading to an improved ability of the CIL to reduce work function and improve electron transporting capability. Moreover, the introduction of the non-ionic OEG chain effectively improve the wetting property and solvent resistance of PDI polymers, so the PPDINN CIL can withstand diverse processing conditions in fabricating different OSCs, including conventional, inverted and blade-coated devices. The binary OSC with conventional structure using PPDINN CIL showed a PCE of 18.6 %, along with an improved device stability. Besides, PPDINN is compatible with the large-area blade-coating technique, and a PCE of 16.6 % was achieved in the 1-cm^2 OSC where a blade-coated PPDINN was used.

[*] L. Feng,[+] Y. Xiang,[+] Z. Li, Q. Li, S. Yan, B. Xu
State Key Laboratory of Chemical Resource Engineering, College of Materials Science and Engineering, Beijing University of Chemical Technology, Beijing, 100029, P. R. China
E-mail: xubowei@buct.edu.cn

J. Hou
State Key Laboratory of Polymer Physics and Chemistry, Beijing National Laboratory for Molecular Sciences, Institute of Chemistry, Chinese Academy of Sciences, Beijing, 100190, P. R. China
E-mail: hjhzlz@iccas.ac.cn

H. Dong
Center for High Pressure Science and Technology Advanced Research, Pudong, Shanghai 201203, P.R. China

J. Hou
University of Chinese Academy of Sciences, Beijing, 100049, P. R. China

[+] These authors contributed equally to this work

Introduction

Organic solar cells (OSCs) have demonstrated tremendous potential as the next-generation photovoltaic technology, with their attractive features such as low cost, portability, solution processing and mechanical flexibility.[1–5] To date, the power conversion efficiencies (PCEs) of state-of-the-art OSCs have exceeded 19 %, reaching the threshold of practical use.[6–9] As a critical component in OSCs, the cathode interlayer (CIL) between the active layer and the cathode metal plays an important role in improving PCE and stability of OSCs.[10–11] Unfortunately, synchronously optimizing the solution-processibility, film-forming ability and solvent resistance of CILs has long been considered as a contradiction, so hardly can any CIL withstand diverse processing conditions in the fabrication of OSCs with different structures.[12–13] This severely limit the application range of CIL materials. For instance, as a predominantly used CIL, inorganic compound ZnO has to be processed through aqueous solution, which excludes its applications in conventional OSCs due to the inability to deposit aqueous solutions onto the organic active layer during device fabrication.[14–16] Besides, although CILs based on organic small molecules and conjugated polymers exhibited high performance in conventional OSCs, they cannot survive from the processing conditions of inverted OSCs because of their poor solvent resistant.[17–20] Furthermore, many CILs displayed significant capability to achieve high PCEs in OSCs, but they only worked well in a thickness of several nanometers owing to the inferior charge transport performance; this excludes their compatibility with high-throughput printing techniques where certain thickness variation is unavoidable.[21–24] From the aspects of industrial production and commercial use, in addition to the capability of achieving high photovoltaic performances, a standard CIL that can be universally used in fabricating diverse OSCs is strongly desired. However, the design of universal CIL materials with excellent electron collection ability, ideal solution-processibility and high solvent resistance is great challenging.

In recent years, organic semiconductors demonstrated great advantages in serving as CILs. With rational molecular design, the organic semiconductors can exhibit a breakthrough conductivity of more than 2000 S·cm^{-1}, displaying promising perspective in serving as CILs.[25–26] Among various organic semiconductors, perylene-diimide (PDI)-

based materials have become the most predominantly used CILs in OSCs due to their suitable energy level, excellent charge transport properties and superior solution-processibility.[27–28] The PDI-based CIL materials are mainly divided into three catalogues: small molecules, conjugated polymers, and non-conjugated polymers. Many PDI-based small molecules such as PDINO,[19] PDINN[29] and PDINN-F[30] were designed and synthesized as CILs in OSCs. Although the PDI small molecules exhibit exceptional capabilities in electron extraction and transportation, the high crystallinity gives rise to strong tendency of aggregation, making them difficult to be fabricated into uniform and smooth CILs.[31] To improve the film-forming ability, the PDI unit was integrated into conjugated polymer backbone. Despite that the PDI conjugated polymers possess efficient charge transport and good film formation, thereby broadening the processing range of CIL thickness, it also causes parasitic absorption which competes with the absorption of the active layers, depressing the PCE of OSCs.[32–33] As an optimization Scheme, non-conjugated polymers of PDI can combine the excellent electrical properties of small molecules with the good film-forming ability of polymers, while maintaining a high optical transmittance of CIL. To date, many non-conjugated PDI polymers, such as PDI-DABC,[34] PPDI-Ac,[35] PDI-50[36] and PDI-PZ,[37] have been developed as CILs that significantly improve the PCE and device stability of OSCs. However, most non-conjugated PDI polymers have to be modified with quaternary ammonium cations in order to achieve adequate water/alcohol solubility. This causes strong polarity, degrading the wetting property of the CIL solution on the active layer surface and leading to poor physical contact at the interface.[38–39] Moreover, the ionic linkages of most PDI-based polymers are only limited to *N*, *N*-dimethyl-substituted ammonium cations, which are subject to degradation through Hofmann eliminations, thereby perturbing the charge distribution and morphology.[34] These issues not only depress the performance of PDI-based CILs, but also restrict their applications. It is promising to design new chemical structure of PDI-based CIL materials, possessing excellent electron collection ability, satisfied solution-processibility and high solvent resistance, for being used in diverse kinds of OSCs including conventional device, inverted device and large-area device.

In this work, we integrated PDI unit in non-conjugated polymer by using a non-ionic oligo (ethylene glycol) (OEG) side chain as linkage to develop two polymeric CILs PPDINN and PPDIN enabling diverse applications in efficient OSCs (Scheme 1). By replacing the ionic mobile counterion-containing linkage with non-ionic OEG, both the doping effect and the film-forming ability of the PDI-based CIL were improved, endowing PPDINN with excellent electron collection capability. Furthermore, the PPDINN solution exhibits good wetting property on the hydrophobic surface of active layer, and the PPDINN film demonstrates high resistance to non-polar organic solvents, thereby enabling it to withstand diverse processing conditions in the fabrication of various OSCs including conventional devices, inverted devices, and large-area devices. The conventional OSC with PPDINN showed an elevated PCE of 18.6 %, along with an improved device stability. The inverted OSC

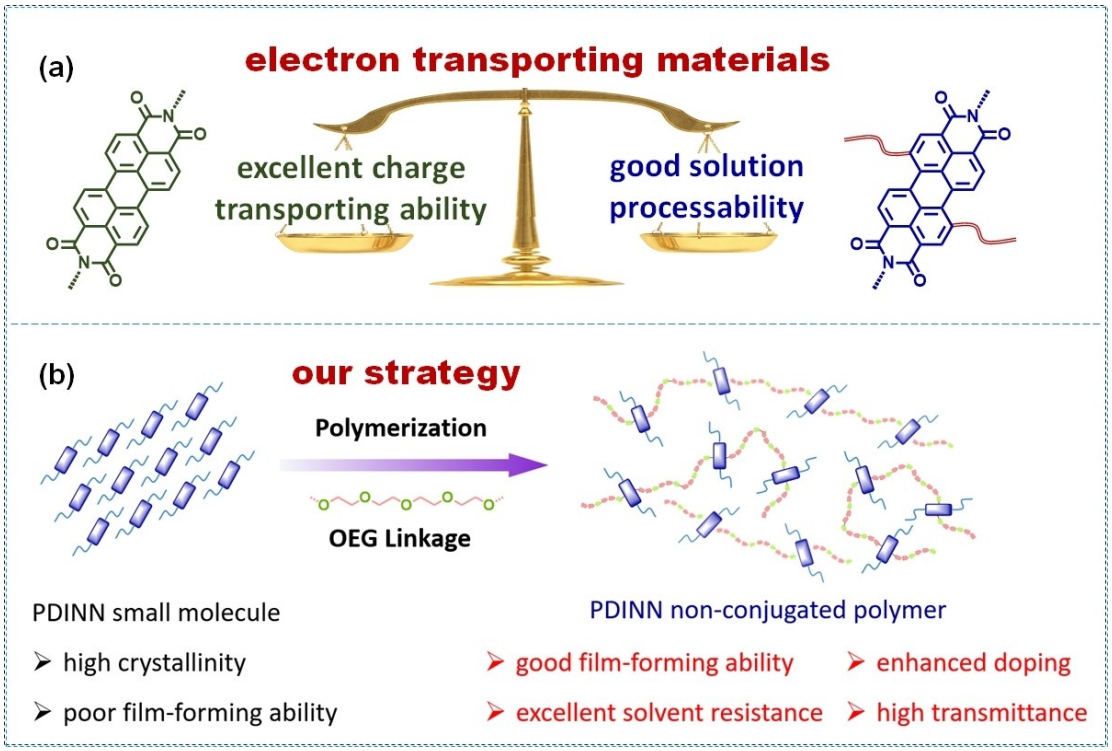

Scheme 1. (a) Advantages of PDI small molecules and PDI polymers as CIL materials; (b) Our strategy for the design of non-conjugated PDI polymers.

modified by PPDINN could exhibit superior PCE to the reference device (16.0% vs. 11.7%), suggesting that PPDINN can serve as a universal CIL for different OSCs. Furthermore, the PPDINN was also compatible with the large-area blade-coating technique, and a PCE of 16.6% was achieved in the 1-cm^2 OSC where a blade-coated PPDINN was used. The results from this work demonstrate that the constructing of non-ionic PDI-based polymers is an effective strategy to develop CILs with good electron collection capability, improved wetting property and adequate solvent resistance, paving the way to explore universal CIL materials for diverse OSCs.

Figure 1a shows the chemical structures of PPDINN, PPDIN and the most well-known high-performing PDINN CIL for comparison. The synthetic routes towards the non-conjugated PDI polymers are outlined in Scheme S1, along with the experimental details. The two ends of OEG chain were firstly linked with benzoic acid groups, which were subsequently modified by boron ester. To prepare the two PDI monomers, perylene-3,4,9,10-tetracarboxylic dianhydride was brominated with 1,3-dibromo-5,5-dimethylhydantoin in the presence of concentrated H_2SO_4. The resulting product then reacted with *N,N*-dimethyldipropylenetriamine and 3-dimethylamino-1-propylamine to yield the two monomers. Suzuki polymerization employing the OEG compound and two bromine-substituted PDI units as monomers yielded the non-conjugated PDI polymers with high molecular weight (number-averaged molecular weights > 15 kDa). The NMR spectra, which confirms the chemical structures of all the intermediates and both PDI polymers, are collected in Supporting Information (Figures S1–S10). The bay substituent of benzoate ester may influence the energy level, molecular packing and solubility of the PDI polymers, which provides great opportunity to improve the electron collection capability of CILs. Both PDI-polymers are soluble in alcohol-based solvents but insoluble in commonly used chlorinated solvents (such as chloroform and chlorobenzene). Such orthogonal solubility with active layer materials is crucial for the multilayer deposition in device fabrication.

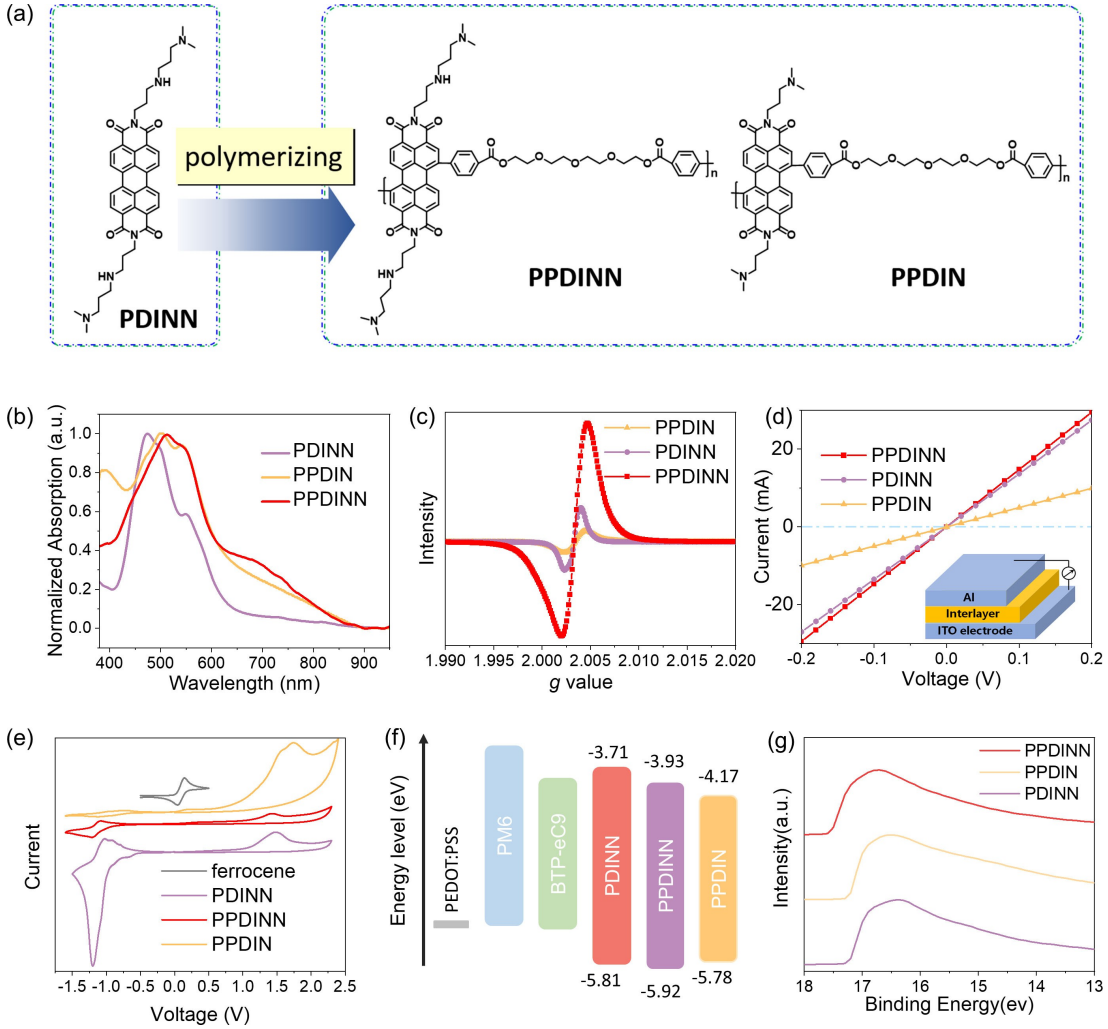

Figure 1. (a) Structure diagram of PPDINN, PPDIN and PDINN; (b) Ultraviolet–visible spectra of PPDINN, PPDIN, PDINN as solid films; (c) ESR spectra of PPDINN, PPDIN, PDINN; (d) *I–V* characteristics of electrical conductivity measurements; (e) CV curves of PPDINN, PPDIN, PDINN; (f) relative positions of the energy levels of different CILs; (g) UPS spectra of PPDINN, PPDIN, PDINN.

The absorption spectra of PPDINN, PPDIN and PDINN in tetrahydrofuran, toluene and *N*,*N*-Dimethylformamide solutions are provided in Figure S10–12 in the Supporting Information. The absorption peaks at ~526 and ~490 nm typically originate from 0–0 and 0–1 transitions of PDI unit. A broad band with low resolved vibronic fine structure ranging from 550 to 700 nm is found in the PPDINN absorption, which is often observed in the bay-substituted PDI molecules.[40–41] The broad band may arise from the combined effect of changes in conjugation length, electron density, and core-twist of the PDI backbone. As shown in Figure 1b, the absorption spectra of the PDI-based CILs as solid films displayed broader bands compared to their solution spectra, owing to the strong solid-state packing of the PDI core.[41–42] Electron spin resonance (ESR) measurements were carried out to probe free radical species in the films. All the samples showed obvious ESR signals, confirming the existence of unpaired electrons (Figure 1c). Since absorption bands related to radical anion were not observed in the spectra, the ESR signals can reflect the electron transfer from the amino pendant to the PDI core. Moreover, the PPDINN displayed a more pronounced ESR signal than PPDIN and PDINN, indicating an enhanced electron transfer process. As is well-known, the free radicals in self-doping semiconductors could effectively improve the electrical conductivity of the materials. Therefore, the conductivities of PPDINN and its small-molecule counterpart PDINN were evaluated by measuring the current–voltage (*I*–*V*) characteristics of the sandwiched devices. As shown in Figure 1d, the conductivities of PPDINN and PDINN were estimated to be 4.97×10^{-3} and 3.64×10^{-3} S/m, respectively. The values of relative dielectric constant (ε_r) were determined to be 3.29, 3.01and 2.99 at 10^4 Hz for PDINN, PPDINN and PPDIN, respectively. The results indicate that the introduction of OEG have negligible influence on ε_r value.

Cyclic voltammetry measurements were performed to experimentally estimate the LUMO energy level (E_{LUMO}) and HOMO energy level (E_{HOMO}) of the CILs. Figure 1e shows the cyclic voltammograms of the PDI derivatives. The E_{LUMO} values were calculated as −3.93, −4.17, and −3.71 eV for PPDINN, PPDIN, and PDINN, respectively (Table 1). The polymer PPDINN showed relatively lower LUMO level, which should be attributed to the electron-withdrawing effect of phenyl carboxylate ester group. Figure 1f presents the energy level diagram of the PDI derivatives and the representative active layer PM6:BTP-eC9. The LUMO energy level of PPDINN is very close to that of the electron acceptors, which can lead to better energy level alignment at the cathode interface for electron transport. From cyclic voltammograms, the E_{HOMO} values are determined to be −5.93, −5.78, and −5.81 eV for PPDINN, PPDIN, and PDINN, respectively. The low-lying E_{HOMO} levels mean that the PDI-based CILs will sufficiently block holes from electron donors. Ultraviolet photoelectron spectroscopy (UPS) was used to probe the work function (WF) values of ITO electrode and the three PDI-based CILs (Figure 1g). The WF of ITO electrode was 4.4 eV, and was reduced to 3.86, 3.96 and 3.99 eV after being covered with PPDINN, PPDIN, and PDINN, respectively. Such a WF reduction of the cathode electrode is essential to achieve ohmic contact at the CIL/active layer interface.

Table 1: Optoelectronic properties of PPDINN, PPDIN and PDINN.

	Conductivity ($S\,m^{-1}$)	LUMO (eV)	HOMO (eV)	Work function (eV)
PPDINN	4.97×10^{-3}	−3.93	−5.93	3.86
PPDIN	1.53×10^{-3}	−4.17	−5.78	3.96
PDINN	3.64×10^{-3}	−3.71	−5.81	3.99

As is well-known, the wetting characteristic, film-forming ability and morphology of CIL not only influence the electron collection capability, but also have considerable impact on physical contact at the interface, which is essential to reduce the interfacial defects. Thus, we firstly investigated the wetting property of the CIL solution on the hydrophobic surface of active layer. As shown in Figure 2a, the methanol solution drop was immediately spread with the contact angle of 28.9° when it contacted the PM6:BTP-eC9 surface, indicating the complete wetting of PPDINN solution on the active layer. To gain insights into the difference of film formation process between polymer PPDINN and its small molecule counterpart PDINN, in situ UV-vis absorption spectra were performed. The time-dependent contour maps of in situ UV-vis absorption spectra were provided in Figure 2b–c & S17. Figure 2b and c showed the time evolution of the UV-vis absorption spectra of PPDINN and PDINN films. Both films exhibited obvious decline in peak intensity, which is typically caused by the decrease in the liquid film thickness. The decline in absorption intensity for PDINN is larger than that for PPDINN, suggesting a greater thickness variation in the PDINN liquid film due to the stronger mobility of small molecule. In the later stage of film formation, the absorption intensity for both PDINN and PPDINN films was recovered, which is originated from molecular aggregation. Throughout the entire film formation process, no shift in absorption peaks was observed for both PDINN and PPDINN films, indicating that the molecular packing arrangement remained unchanged during the film formation. To elucidate the crystallinity and molecular packing of the PDI-based CILs, we employed grazing incidence wide-angle X-ray scattering (GIWAXS) measurements. The 2D GIWAXS patterns for PDINN and PPDINN are illustrated in Figure 2d and e. It can be clearly observed that, in the out-of-plane (OOP) directions, the π–π stacking diffraction peaks for the polymer PPDINN were remarkably weakened, compared to its small-molecule counterpart PDINN. This indicates a lower crystallinity of the PDI-based polymer. Particularly, the PPDINN film showed GIWAXS patterns with the lamellar (100) packing in the in-plane (IP) directions and π–π stacking (010) peaks in the OOP direction, indicating the preferential formation of the face-on orientation, which is beneficial for charge transport. The π–π stacking distance of 3.6 Å remained almost unchanged between PDINN and PPDINN (Figure 2f and g). X-ray diffraction (XRD) measurements were used to reveal the crystallinity of the PDI films (Figure S18). A

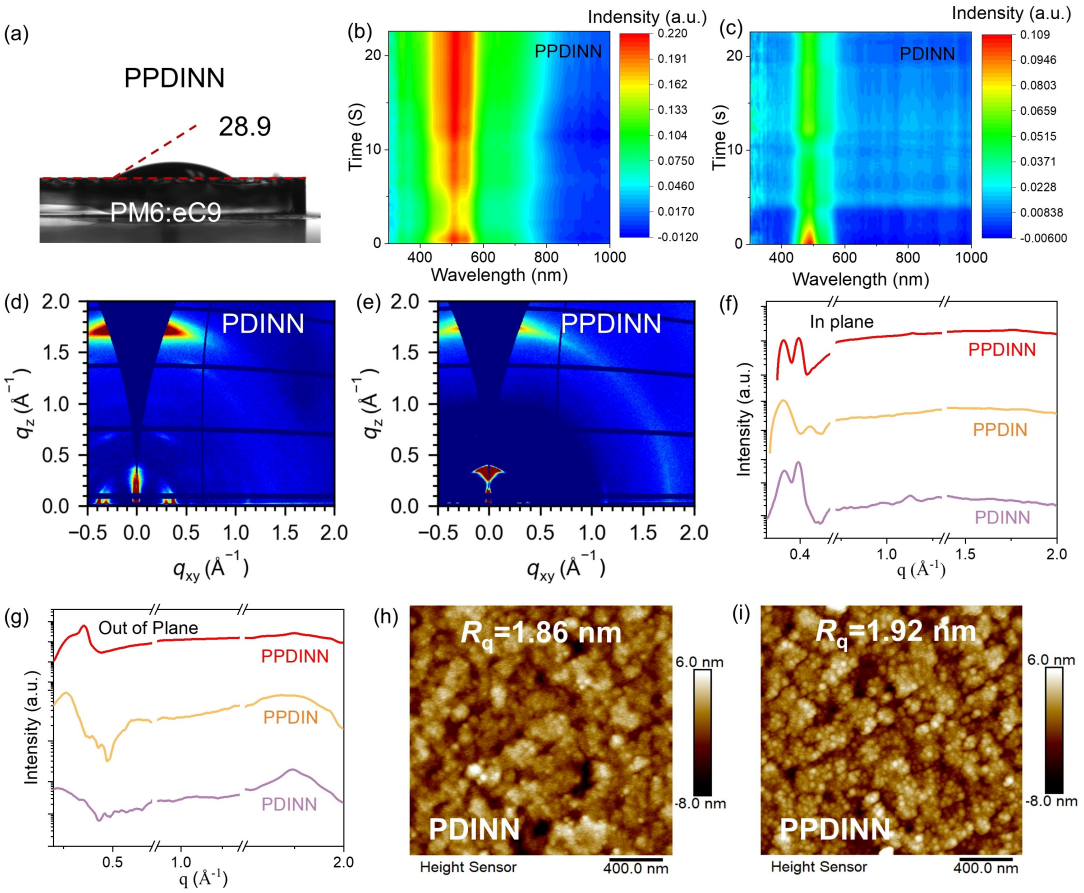

Figure 2. (a) Contact angle of PPDINN dissolved in methanol on active layer surface; the time-dependent contour maps of in situ UV-vis absorption spectra of (b) PPDINN and (c) PDINN; The 2D GIWAXS pattern of (d) PDINN and (e) PPDINN neat films; In-plane line-cut (f) and out-of-plane line-cut (g) profiles of PPDINN, PDINN and PPDIN neat films; atomic force microscopy height images of ITO electrodes covered by (h) PDINN and (i) PPDINN.

pronounced diffraction peak at 2θ = 25.7° was observed in the PDINN film, corresponding to a π–π stacking distance of 3.5 Å, which is in good agreement with the results from GIWAXS. In contrast, owing to the low crystallinity of the non-conjugated polymers, no clear peak could be observed in the diffraction pattern of PPDINN and PPDIN films. Only broad and uninformative signals in the 2θ region of 10°-30° were found in the PPDINN and PPDIN samples. Surface morphologies of the CILs were investigated by tapping-mode atomic force microscopy (AFM), as shown in Figure 2h–i & S20. The root-mean-square roughness (R_q) values of PDINN and PPDINN films were all around 1.9 nm. The smooth surface of the CILs can passivate the interfacial defects, which is favorable for decreasing the leakage current of the devices. Therefore, the face-on molecular arrangement, the tight π–π stacking and the smooth surface will improve the capability of PPDINN in electron transport.

To investigate the performance of PPDINN and PPDINN as CILs, OSCs with the conventional structure ITO/PEDOT:PSS/PM6:BTP-eC9/CIL/Ag were fabricated (Figure 3a). The optimal thickness of the PDI CILs is ~10 nm, and the optimization process for CIL thickness is summarized in Table S3. The blend of PM6:BTP-eC9 was used as the active layer. The current density-voltage (*J–V*) curves and corresponding photovoltaic parameters are shown in Figure 3b and Table 2. Benefiting from the low WF and excellent conductivity, the OSC with the PPDINN CIL exhibited a PCE of 18.59 %, along with an open-circuit voltage (V_{oc}) of 0.873 V, a current density (J_{sc}) of 27.32 mA·cm^{-2}, and a fill factor (FF) of 77.9 %. The PCE of the OSC device with PPDINN is higher than that of the reference device modified by PDINN (PCE = 18.1 %). Subsequently, a total of 20 independent devices from five batches were fabricated to assess the performance reproducibility. Figure S30 displays the statistical distribution of the photovoltaic efficiencies for OSCs with PPDINN and PDINN. The PCE values of the PPDINN-modified OSCs exhibited a narrower distribution compared to those of the

Table 2: Photovoltaic performances of the OSCs.

	V_{oc} (V)	J_{sc} (mA/cm^2)	J_{Cal} (mA/cm^2)	FF (%)	PCE (%)
PDINN	0.870	27.33	26.72	76.10	18.09
PPDINN	0.873	27.32	26.81	77.93	18.59

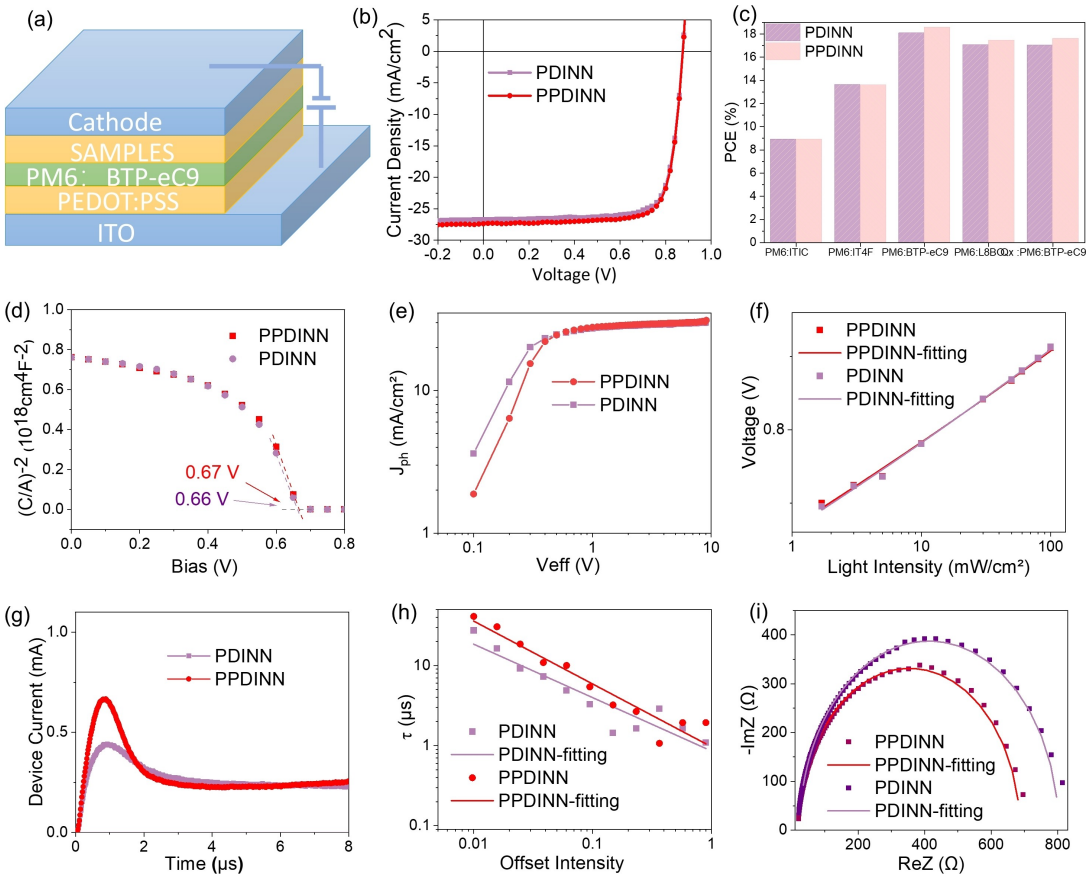

Figure 3. (a) Configuration of the OSCs fabricated in this study ; (b) *J–V* curves of the OSCs using PPDINN and PDINN; (c) PCE values for OSCs with the active layers of PM6:ITIC, PM6:IT4F, PM6:BTP-eC9, PM6:L8BO, and PBQx-TCl:PM6:eC9-2Cl; (d) Mott–Schottky analyses for the OSCs; (e) characteristics of exciton dissociation probabilities for the OSCs; (f) V_{oc}-light intensity relationship for the OSC devices; (g) photo-CELIV for the OSCs with PPDINN and PDINN; (h) characterization of charge–carrier lifetime; (i) Nyquist plots of impedance spectra of the OSCs based on PPDINN and PDINN.

PDINN devices. Compared to PDINN, the PPDINN-based OSCs exhibit better performance reproducibility, which is conducive to promoting the yield during large-scale production. The superior repeatability of PPDINN-modified OSCs may be derived from the lower HOMO level and the higher conductivity of PPDINN. As reported in many previous works, the low-lying HOMO level is favorable for hole-blocking, and the high conductivity can effectively suppress the charge recombination. Consequently, the PPDINN CIL can deliver stable performance even with thickness variation. Table S3 shows the influence of CIL thicknesses on OSC performances. A PCE of 17.6 % can be achieved even when the PPDINN thickness was increased to 40 nm. The excellent film thickness tolerance might be responsible for the good repeatability of PPDINN-based OSCs. These results suggest that PPDINN outperforms its small-molecule counterpart PDINN in the fabrication of efficient OSCs. The constructing of non-conjugated PDI polymer by using non-ionic linkage can be an effective approach to develop high-performance CIL materials. Furthermore, the universality of PPDINN is demonstrated by fabricating the OSCs with other representative active layers, such as PM6:IT4F, PM6:ITIC, PBQx-TCl:PM6:eC9-2Cl, and PM6:L8BO (Figure 3c). As shown in Table S4, all the PPDINN-based OSCs exhibited higher PCEs compared to the reference devices modified by PDINN. The results indicate that PPDINN can be used in various OSCs with different active layers.

The charge dynamics of the OSCs was studied to reveal the superior electron transport capability of PPDINN. The built-in voltage (V_{bi}) of devices was estimated by means of Mott–Schottky analysis, and the V_{bi} of PPDINN-based OSCs is 0.67 V which is comparable to that of the PDINN device (0.66 V), as shown in Figure 3d. The high V_{bi} value indicates that the ideal internal electric field can be achieved, thereby realizing an excellent electron collection efficiency in the PPDINN-based OSC.[43] The exciton dissociation probabilities (P_{diss}) of OSC devices are calculated to be 97 % for PPDINN and 96 % for PDINN, respectively (Figure 3e). Also, we studied the dependence of V_{oc} on light intensity (P_{light}), and the PPDINN-modified OSCs exhibit a slope of 1.02 K_BT/q, indicating that the trap-assisted recombination is suppressed in the device (Figures 3f). Moreover, the slope of the J_{sc} versus P_{light} plot for the PPDINN cell is close to unity ($\alpha = 1$), suggesting a negligible bimolecular recombination (Figures S23). As shown in Fig-

ure 3g, the charge carrier mobility of the OSCs was investigated by using photo-induced charge-carrier extraction by a linearly increasing voltage (Photo-CELIV). The mobilities of OSCs with PPDINN and PDINN are 2.83×10^{-4} and 2.67×10^{-4} $cm^2V^{-1}s^{-1}$, respectively. Moreover, as presented in Figure 3h, the results of transient photovoltage measurements indicate that the charge carrier lifetime of the PPDINN device is 0.96 μs, which is longer than that of the PDINN device (0.86 μs). The above results imply that the non-conjugated polymer possess superior carrier extraction and transport capabilities to its small-molecule counterpart PDINN, contributing to the high FF of the OSC device. To estimate the interfacial resistances of the OSCs, electrochemical impedance spectroscopy (EIS) was performed and the measured Nyquist plots were fitted by using an equivalent circuit model (Figure 3i).[44] The series resistance (R_s) values were 0.89 $\Omega\cdot cm^2$ for the PPDINN device and 0.86 $\Omega\cdot cm^2$ for the PDINN device. The characterization results of semiconductor devices demonstrated the good electron transporting capability of PPDINN, which is essential to diminish the charge recombination, so as to achieve high FF and PCE in OSCs.

Transient absorption (TA) spectra of the bilayers with different PDI-based CILs were measured to investigate the charge transfer dynamics at the CIL/active layer interface. Figure 4a and b displayed 2D color plots for the bilayers PDINN/PM6:BTP-eC9 and PPDINN/PM6:BTP-eC9, while the results for PPDIN/PM6:BTP-eC9 and blank/PM6:BTP-eC9 bilayers were presented in Figure S29. Common bleach peaks, representing ground-state bleaching (GSB) of PM6 and BTP-eC9, were observed at 560–660 nm and 800–860 nm across all samples.[45] Figure 4c–d highlights the temporal progression of exciton and charge dynamics, as extracted from the TA spectra. The GSB signal of BTP-eC9 for the PPDINN-based bilayer exhibited a fast decay. Figure 4f illustrates the transient kinetics of GSB signals at 840 nm for the blank, PDINN, PPDIN and PPDINN samples, revealing the processes of exciton and electronic excitation population and depopulation associated with electron transfer.[46–47] Compared to the PM6:BTP-eC9 layer without CIL, both the PDINN- and PPDINN-based samples exhibit rapid decay rates for the GSB signal of BTP-eC9, suggesting the efficient electron transfer from active layer to the CILs. The above results suggest that efficient utilization of excitons and enhanced electron transfer can be realized by incorporating the PPDINN CIL.

To demonstrate the universality of PPDINN in OSCs, the application of PPDINN in inverted OSCs was explored by fabricating OSC devices with an inverted configuration of ITO/CIL/PM6:BTP-eC9/MoO_3/Al. To evaluate the capacity of PPDINN in fabricating inverted OSCs, we firstly investigate the solvent resistance of the PDI-based CILs. As shown in Figure S24, the absorption intensity of the PPDINN film remains almost unchanged after the PPDINN film is washed by chloroform, implying that PPDINN can resist the solvent corrosion in the fabrication of inverted OSC device. In contrast, the absorption band of PDINN disappears completely owing to its better solubility. As listed in Table S5, the inverted OSC modified by PPDINN was fabricated, showing a PCE of 16.0 %, which is remarkably higher than that of the reference device with PDINN (PCE = 11.7 %). The superior performance of PPDINN to its small-molecule counterpart PDINN in fabricating inverted OSCs suggests that constructing non-conjugated polymers can provide an effective way to broaden the application range of PDI-based CILs. Afterwards, we evaluated the compatibility of PPDINN with large-area blade-coating techniques. As shown in Figure 5c, the 1-cm^2 PPDINN film prepared through blade-coating exhibits a low R_q of 2.21 nm, which is similar to the spin-coated film.

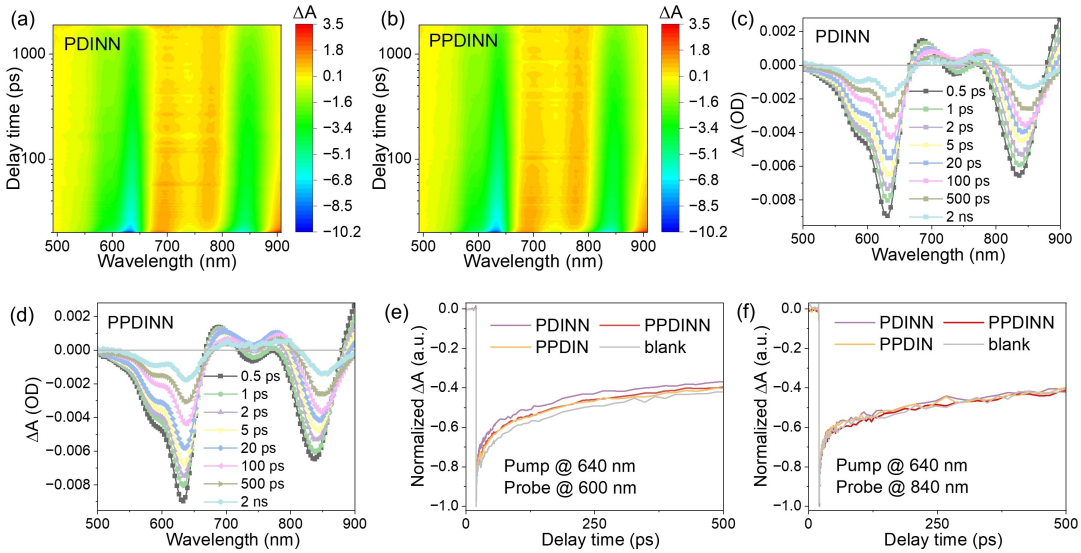

Figure 4. 2D TA color plots of the bilayer (a) PDINN/PM6:BTP-eC9 and (b) PPDINN/PM6:BTP-eC9 films, excited at 640 nm; TA spectra of the bilayer films of (c) PDINN/PM6:BTP-eC9 and (d) PPDINN/PM6:BTP-eC9; and Normalized kinetic traces of the bilayers with PPDINN, PDINN, PPDIN layers probed at (e) 600 and (f) 840 nm.

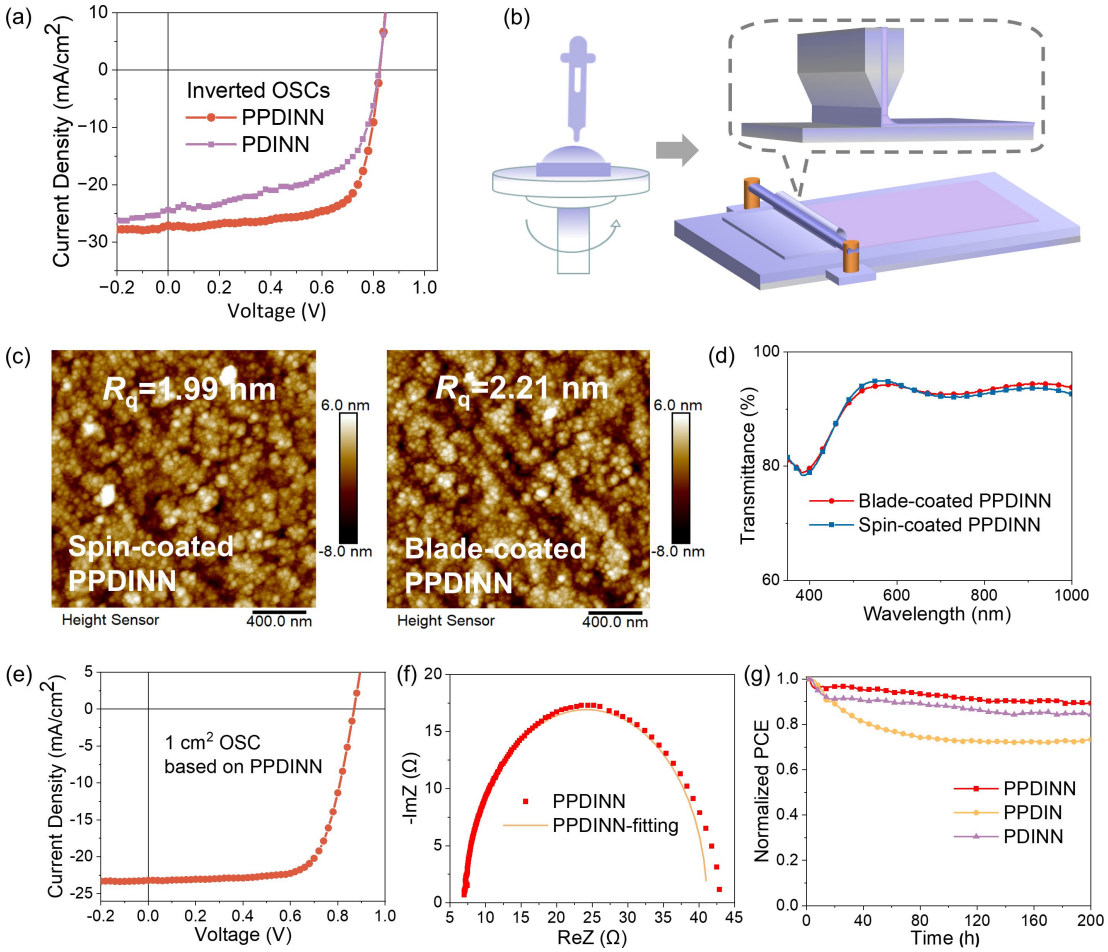

Figure 5. (a) *J–V* curves of the inverted OSCs using PPDINN and PDINN; (b) Schematic diagram of blade-coating processing; (c) AFM height images of spin-coated and blade-coated PPDINN on ITO glass; (d) Transmittance spectra; (e) Photovoltaic characteristic of 1 cm^2 OSC device; (f) Nyquist plots of impedance spectrum of the 1 cm^2 OSC based on PPDINN; (g) Normalized PCE values as a function of storage time under simulated sunlight (AM 1.5 G) for PPDINN- and PDINN-based devices.

Meanwhile, the absorption spectrum of the blade-coated PPDINN film exhibits a high transmittance (Figure 5d), which can ensure the sufficient light-harvesting of the active layer. The 1-cm^2 OSC was fabricated by using a blade-coated PPDINN film as CIL, showing a PCE of 16.65 % (Figure 5e). The decline in PCE for the 1 cm^2 OSC, as compared to the small-area device, should be ascribed to the increased R_s (6.21 $\Omega \cdot cm^2$), as shown in Figure 5f. The above results imply that PPDINN is compatible with large-area processing techniques, making it a promising CIL for practical application. The operational stability of the OSCs is highly concerned in their practical use because they are supposed to work under sunlight illumination. Thus, the stability of the devices under simulated sunlight (AM 1.5 G) was investigated. As shown in Figure 5g, the PCE of PPDINN-based OSC maintained 89 % of its initial value after continuous illumination for 200 h. Meanwhile, the devices with PDINN and PPDIN retained 85 % and 73 % of their performances, respectively. These results demonstrate the good intrinsic and operational stabilities of the PPDINN-modified OSCs. Besides the photovoltaic efficiency, the intrinsic stability and operational stability of the OSCs are also evaluated. The OSCs are encapsulated and stored in air at room temperature. As shown in Figure S26, the device modified by PPDINN maintained 89 % of the initial PCE value after a storage of 30 days while the PDINN-based device only preserved 85 % of its original efficiency. Additionally, the OEG chain does not contain any mobile counterion, which is favorable to the improvement of device stability.

In conclusion, we designed and synthesized a non-ionic PDI polymer PPDINN that can be used as CILs in diverse types of OSCs. The introduction of OEG enhance the n-doping effect of the PDI polymer, leading to an enhanced ability of the CIL to reduce WF and improve electron transporting capability; this effectively upgrades the electron collection ability of PDI-based CIL. Moreover, the utilizing of non-ionic OEG chain to replace the commonly used ammonium-containing polar groups endows the non-conjugated PDI polymer with improved wetting property and adequate solvent resistance, so the PPDINN CIL can withstand diverse processing conditions in the fabrication of

OSCs with different structures, including conventional, inverted and blade-coated devices. By using PPDINN as CIL, OSC with conventional structure showed an elevated PCE of 18.6 %, along with an improve device stability. Moreover, PPDINN also demonstrated superior performance in cathode modification to its small-molecule counterpart PDINN in inverted OSCs (16.0 % vs. 11.7 %). Besides, PPDINN is compatible with the large-area blade-coating technique, and a PCE of 16.6 % was achieved in the 1-cm^2 OSC where a blade-coated PPDINN was used.

Acknowledgements

We appreciate the kindly help from Prof. Zhengrong Wei and Dr. Yuan Cheng in Hubei University on transient absorption measurement. B.X. would like to acknowledge the financial support from Fundamental Research Funds for the Central Universities (buctrc202140). The authors acknowledge the National Natural Science Foundation of China (No. 52273166) and Beijing Municipal Science & Technology Commission (2242013).

Conflict of Interest

The authors declare no conflict of interest.

Data Availability Statement

Research data are not shared.

Keywords: Organic solar cells · perylene-diimide polymer · crystallinity · solvent resistance · molecular packing

[1] A. J. Heeger, *Adv. Mater.* **2014**, *26*, 10–28.
[2] X. Du, T. Heumueller, W. Gruber, A. Classen, T. Unruh, N. Li, C. J. Brabec, *Joule* **2019**, *3*, 215–226.
[3] A. Sandstrom, H. F. Dam, F. C. Krebs, L. Edman, *Nat. Commun.* **2012**, *3*, 1002.
[4] T. T. Larsen-Olsen, R. R. Søndergaard, K. Norrman, M. Jørgensen, F. C. Krebs, *Energy Environ. Sci.* **2012**, *5*, 9467–9471.
[5] H. Li, Z. Zheng, S. Yang, T. Wang, Y. Yang, Y. Tang, S. Zhang, J. Hou, *Adv. Mater.* **2024**, *36*, 2311476.
[6] L. Zhou, H. Yu, J. Zhang, D. Qiu, Y. Fu, J. Yi, L. Xie, X. Li, L. Meng, J. Zhang, X. Lu, Z. Wei, Y. Li, H. Yan, *Angew. Chem. Int. Ed.* **2024**, *63*, e202319635.
[7] H. Zhang, G. Ran, X. Cui, Y. Liu, Z. Yin, D. Li, X. Ma, W. Liu, H. Lu, R. Liu, L. Cai, W. Zhang, S. Guo, H. Li, J. Yu, Y. Lin, Y. Liu, G. Lu, Z. Ma, P. Cheng, Z. Bo, *Adv. Energy Mater.* **2023**, *13*, 2302063.
[8] L. Wang, C. Chen, Y. Fu, C. Guo, D. Li, J. Cheng, W. Sun, Z. Gan, Y. Sun, B. Zhou, C. Liu, D. Liu, W. Li, T. Wang, *Nat. Energy* **2024**, *9*, 208–218.
[9] J. Yuan, Y. Zhang, L. Zhou, G. Zhang, H.-L. Yip, T.-K. Lau, X. Lu, C. Zhu, H. Peng, P. A. Johnson, M. Leclerc, Y. Cao, J. Ulanski, Y. Li, Y. Zou, *Joule* **2019**, *3*, 1140–1151.
[10] Z. C. He, H. B. Wu, Y. Cao, *Adv. Mater.* **2014**, *26*, 1006–1024.
[11] Z. Yin, J. Wei, Q. Zheng, *Adv. Sci.* **2016**, *3*, 1500362.
[12] Y. Yang, J. Wang, P. Bi, Q. Kang, Z. Zheng, B. Xu, J. Hou, *Chem. Mater.* **2022**, *34*, 6312–6322.
[13] H. Wang, Y. Yang, Y. Zhang, S. Wang, Z. a Tan, S. Yan, L. Wang, J. Hou, B. Xu, *Adv. Funct. Mater.* **2023**, *33*, 2213914.
[14] Y. Wang, Z. Zheng, J. Wang, X. Liu, J. Ren, C. An, S. Zhang, J. Hou, *Adv. Mater.* **2022**, *35*, e2208305.
[15] X. Liu, Z. Zheng, J. Wang, Y. Wang, B. Xu, S. Zhang, J. Hou, *Adv. Mater.* **2021**, *34*, e2106453.
[16] L. Nian, K. Gao, F. Liu, Y. Y. Kan, X. F. Jiang, L. L. Liu, Z. Q. Xie, X. B. Peng, T. P. Russell, Y. G. Ma, *Adv. Mater.* **2016**, *28*, 8184–8190.
[17] Z. Wu, C. Sun, S. Dong, X.-F. Jiang, S. Wu, H. Wu, H.-L. Yip, F. Huang, Y. Cao, *J. Am. Chem. Soc.* **2016**, *138*, 2004–2013.
[18] T. Dai, X. Li, Y. Zhang, X. Zhou, Y. Zhu, J. Zhou, D. Xu, T. Lin, *Solar RRL* **2021**, *5*, 2100151.
[19] Z.-G. Zhang, B. Qi, Z. Jin, D. Chi, Z. Qi, Y. Li, J. Wang, *Energy Environ. Sci.* **2014**, *7*, 1966.
[20] J. X. Han, Y. C. Chen, W. P. Chen, C. Z. Yu, X. X. Song, F. H. Li, Y. Wang, *ACS Appl. Mater. Interfaces* **2016**, *8*, 32823–32832.
[21] X. Ouyang, R. Peng, L. Ai, X. Zhang, Z. Ge, *Nat. Photonics* **2015**, *9*, 520–524.
[22] H. Liu, Z. X. Liu, S. Wang, J. Huang, H. Ju, Q. Chen, J. Yu, H. Chen, C. Z. Li, *Adv. Energy Mater.* **2019**, *9*, 1900887.
[23] S. Ohisa, M. Suzuki, T. Chiba, J. Kido, *ACS Appl. Mater. Interfaces* **2019**, *11*, 25351–25357.
[24] K. Zhang, B. Fan, R. Xia, X. Liu, Z. Hu, H. Gu, S. Liu, H.-L. Yip, L. Ying, F. Huang, Y. Cao, *Adv. Energy Mater.* **2018**, *8*, 1703180.
[25] H. Tang, Y. Liang, C. Liu, Z. Hu, Y. Deng, H. Guo, Z. Yu, A. Song, H. Zhao, D. Zhao, Y. Zhang, X. Guo, J. Pei, Y. Ma, Y. Cao, F. Huang, *Nature* **2022**, *611*, 271–277.
[26] H. Tang, Y. Bai, H. Zhao, X. Qin, Z. Hu, C. Zhou, F. Huang, Y. Cao, *Adv. Mater.* **2023**, *36*, 2212236.
[27] W.-Y. Lee, J. H. Oh, S.-L. Suraru, W.-C. Chen, F. Würthner, Z. Bao, *Adv. Funct. Mater.* **2011**, *21*, 4173–4181.
[28] C.-C. Kao, P. Lin, Y.-Y. Shen, J.-Y. Yan, J.-C. Ho, C.-C. Lee, L.-H. Chan, *Synth. Met.* **2008**, *158*, 299–305.
[29] J. Yao, B. Qiu, Z. G. Zhang, L. Xue, R. Wang, C. Zhang, S. Chen, Q. Zhou, C. Sun, C. Yang, M. Xiao, L. Meng, Y. Li, *Nat. Commun.* **2020**, *11*, 2726.
[30] J. Yao, S. Ding, R. Zhang, Y. Bai, Q. Zhou, L. Meng, E. Solano, J. A. Steele, M. B. J. Roeffaers, F. Gao, Z. G. Zhang, Y. Li, *Adv. Mater.* **2022**, *34*, e2203690.
[31] Q. Kang, L. Ye, B. Xu, C. An, S. J. Stuard, S. Zhang, H. Yao, H. Ade, J. Hou, *Joule* **2018**, *3*, 227–239.
[32] C. Sun, Z. Wu, Z. Hu, J. Xiao, W. Zhao, H.-W. Li, Q.-Y. Li, S.-W. Tsang, Y.-X. Xu, K. Zhang, H.-L. Yip, J. Hou, F. Huang, Y. Cao, *Energy Environ. Sci.* **2017**, *10*, 1784–1791.
[33] C. Zhu, J. Tian, W. Liu, Y. Duan, Y. Song, Z. You, X. Wang, N. Li, X. Zhan, T. P. Russell, Y. Liu, *ACS Energy Lett.* **2023**, *8*, 2689–2698.
[34] Z. You, Y. Song, W. Liu, W. Wang, C. Zhu, Y. Duan, Y. Liu, *Angew. Chem. Int. Ed.* **2023**, *62*, e202302538.
[35] Z. Hu, R. Xu, S. Dong, K. Lin, J. Liu, F. Huang, Y. Cao, *Mater. Horiz.* **2017**, *4*, 88–97.
[36] Y. Liu, M. D. Cole, Y. Jiang, P. Y. Kim, D. Nordlund, T. Emrick, T. P. Russell, *Adv. Mater.* **2018**, *30*, 1705976.
[37] Y. Liu, M. Sheri, M. D. Cole, T. Emrick, T. P. Russell, *Angew. Chem. Int. Ed.* **2018**, *57*, 9675–9678.
[38] M. Liu, P. Fan, Q. Hu, T. P. Russell, Y. Liu, *Angew. Chem. Int. Ed.* **2020**, *59*, 18131–18135.
[39] M. Liu, Y. Jiang, D. Liu, J. Wang, Z. Ren, T. P. Russell, Y. Liu, *ACS Energy Lett.* **2021**, *6*, 3228–3235.
[40] T. L. H. Mai, S. Jeong, S. Kim, S. Jung, J. Oh, Z. Sun, J. Park, S. Lee, W. Kim, C. Yang, *Adv. Funct. Mater.* **2023**, *33*, 2303386.

[41] J. Jia, B. Fan, M. Xiao, T. Jia, Y. Jin, Y. Li, F. Huang, Y. Cao, *Macromolecules* **2018**, *51*, 2195–2202.
[42] W. J. Sun, Y. T. Wang, Y. Zhang, B. Sun, Z. Q. Zhang, M. J. Xiao, X. Y. Li, Y. Huo, J. Xin, Q. Zhu, W. Ma, H. L. Zhang, *Angew. Chem. Int. Ed. Engl.* **2022**, *61*, e202208383.
[43] H. Zhou, Y. Zhang, J. Seifter, S. D. Collins, C. Luo, G. C. Bazan, T. Q. Nguyen, A. J. Heeger, *Adv. Mater.* **2013**, *25*, 1646–1652.
[44] W. L. Leong, S. R. Cowan, A. J. Heeger, *Adv. Energy Mater.* **2011**, *1*, 517–522.
[45] J. Ren, S. Zhang, Z. Chen, T. Zhang, J. Qiao, J. Wang, L. Ma, Y. Xiao, Z. Li, J. Wang, X. Hao, J. Hou, *Angew. Chem. Int. Ed.* **2024**, e202406153.
[46] K. Zhang, X. Du, J. Qiao, H. Hu, W. Zhang, L. Wang, M. Gao, H. Yin, W. Qin, X. Hao, *Energy Environ. Sci.* **2022**, *15*, 5261–5273.
[47] K. Zhang, Z. Jiang, J. Qiao, P. Lu, C. Qin, H. Yin, X. Du, W. Qin, X. Hao, *Energy Environ. Sci.* **2023**, *16*, 3350–3362.

Manuscript received: June 9, 2024
Accepted manuscript online: July 28, 2024
Version of record online: ■■, ■■

Research Article

Organic Solar Cells

L. Feng, Y. Xiang, Z. Li, Q. Li, H. Dong, S. Yan, B. Xu,* J. Hou* **e202410857**

Non-Ionic Perylene-Diimide Polymer as Universal Cathode Interlayer for Conventional, Inverted, and Blade-Coated Organic Solar Cells

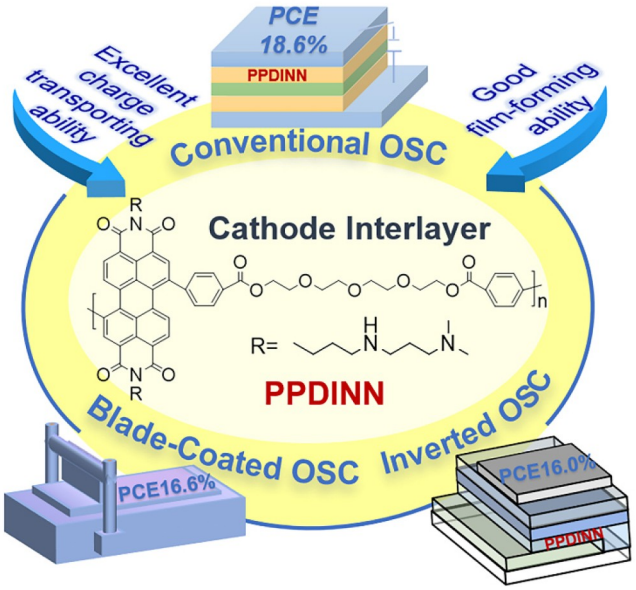

A non-conjugated PDI polymer PPDINN was designed and synthesized by utilizing oligo (ethylene glycol) (OEG) as linkage, exhibiting pronounced n-doping effect, improved film-forming ability and good solvent resistance of the polymer film. By using PPDINN as cathode interlayer, excellent photovoltaic performances were achieved in conventional, inverted and blade-coated organic solar cells.